periodica polytechnica

Chemical Engineering
53/2 (2009) 31–40
doi: 10.3311/pp.ch.2009-2.01
web: http://www.pp.bme.hu/ch

RESEARCH ARTICLE

The influence of the interfacial properties of composite catalyst material on the photocatalytic conversion of TiO_2 layer silicates

Róbert Kun / *Imre* Dékány
Received 2009-05-27

Abstract

Solid-gas and solid-liquid interfacial properties of titanium dioxide/layer silicate composite sorbents were studied by sorption experiments and the photocatalytic properties were also investigated.

The photocatalyst TiO_2 was prepared by the sol-gel method and the sol obtained was used for heterocoagulation of Na-montmorillonite at several different mass ratios, yielding supported photocatalysts of various compositions. The TiO_2 content of the samples ranged from 20 to 75 wt%. The specific surface areas of the samples, determined by nitrogen adsorption, ranged from 120 to 290 m^2/g. The catalytic properties of TiO_2/montmorillonite composites were tested by photo-oxidation of dichloro acetic acid (DCA). The specific surface area and the porosity exert a major influence on the photocatalytic efficiency through the interfacial layer properties. The rate of photo-oxidation of DCA depends strongly on the surface accessibility of the intermediates and the specific surface area calculated from gas and liquid mixture adsorption data. The conversion data of DCA presented show that the photocatalytic efficiency of TiO_2 can depend significantly on the accessibility of different molecules to the TiO_2 nanocrystals embedded in the layer silicate support in confined space.

Keywords

adsorption · liquid mixtures · surface area · porosity · photocatalysis · confined space

Acknowledgement

The authors are very thankful for the financial support of the Hungarian National Scientific Fund OTKA project Nr. K 73307

Róbert Kun

Supramolecular and Nanostructured Materials Research Group, Hungarian Academy of Sciences, 1525 Budapest, P.O.B. 17, Hungary

Imre Dékány

Department of Physical Chemistry and Materials Sciences, University of Szeged, Aradi vt. 1, H-6720 Szeged, Hungary
e-mail: i.dekany@chem.u-szeged.hu

Introduction

The surface properties of solid support materials can strongly influence the interfacial processes at the solid-liquid interface. Catalytic processes occur in the interfacial region in a distance range of 1-2 nm from the solid support material, which means that the adsorption layer structure and composition can influence the rate of the catalytic processes.

We expect that the catalytic properties of layer silicate supported TiO_2 nanoparticles can be predicted from binary liquid adsorption isotherms. The surface of the layer silicate is hydrophilic, because the surface of the silicate layer has a negative charge, which is compensated by sodium cations. Incorporation of TiO_2 nanoparticles into the interlamellar space will modify the surface energy of the clay support material for adsorption processes.

Titanium dioxide is one of the most important photocatalysts, by virtue of its chemical stability and its good light absorption properties. Preparation of TiO_2 has been the subject of a large number of publications [1]-[8]. The majority of these works describes titanium dioxide products prepared by controlled hydrolysis of titanium(IV) alkoxides. In the course of hydrolysis, water is the reaction partner of the titanium precursor and, in most cases, it is also the main component of the reaction medium (alcohol/water mixture). In the various publications, the water content of the reaction medium varies over a wide range, from pure water to a water content corresponding to the stoichiometry of hydrolysis [9]-[16]. Many publications are found in the relevant literature on the preparation and evaluation of composite materials containing titanium dioxide. Supported or composite materials possess more advantageous properties for practical applications than pure titanium dioxide [9]-[12]. Among composite-forming or support materials with hydrophilic or hydrophobic surface characteristics, layer silicates are most widely used [16]-[18]. Sterte et al. performed acid hydrolysis of titanium(IV) chloride. The TiO_2 sol formed was added to montmorillonite suspensions [1]. The products exhibited very low crystallinity; the onset of anatase formation was detected by X-ray diffraction. Typically, the TiO_2 sol prepared under acidic conditions was added to suspensions of Na-montmorillonite and

the structure of the nanocomposite obtained was studied. In all cases highly acidic sol was used (pH < 1.8). The nanocomposites obtained contained amorphous or barely crystalline titanium dioxide. The anatase phase appeared only if the composites were subsequently heat-treated (by hydrothermal procedure or calcination). The pillars are very small, typically 1-2 nm. The extremely large specific surface areas (200-400 m^2/g), considerably reduced by heat treatment, are due to the amorphous structure and the very small particle size [14]-[18].

Photocatalytic oxidation of numerous compounds has been studied on titanium dioxide catalyst. Preferred model compounds have been phenol [18] and its chlorinated derivatives [6], salicylic acid and other carboxylic acid derivatives [19], dye molecules [10], and dichloroacetic acid [20]. Efforts have been made to optimize the accessible catalytic surface of supported and composite catalysts containing titanium dioxide.

The aim of the present work was to prepare, by heterocoagulation, pillared TiO_2/montmorillonite nanocomposites for which the solid-gas and solid-liquid adsorption properties of the composite catalyst materials are known. Using different TiO_2/layer silicate mass ratios, the structure of the composites can be modified systematically. The samples obtained by heterocoagulation, having different specific surface area and porosity and high crystalline anatase content, will be investigated in sorption and photocatalytical experiments.

1 Adsorption of binary liquid mixtures on solid surfaces

When solid particles are immersed in a liquid medium, solid/liquid interfacial interactions will cause the formation of an adsorption layer on their surface. Following D.H. Everett, G. Schay and L.G. Nagy, the sorption exchange process taking place at the solid-liquid interface may be described in thermodynamically exact terms when the activities of the interfacial layer and of the bulk phase are known. In accordance with the exchange equilibrium in binary liquid mixtures at the solid-liquid interface, the liquid sorption equilibrium constant (K) is given by the following formula [21]-[28]:

$$(1) + r(2)^s \rightleftarrows (2)^s + r(2) \tag{1}$$

$$K = \frac{x_1^s \, f_1^s (x_2 \, f_2)^r}{(x_2^s \, f_2^s)^r \, x_1 \, f_1} \tag{2}$$

where x_1^s and x_2^s are the molar fraction of the interfacial layer and x_1 and x_2 that in the bulk liquid phase respectively, f_1^s and f_2^s are the activity coefficients in the interfacial layer and f_1 and f_2 in the bulk liquid. Assuming that $f_1^s/f_2^s \approx 1$, i.e., that the activity coefficients of the interfacial phase compensate for each other [29]-[31], then

$$K' = \frac{x_1^s (a_2)^r}{(x_2^s)^r \, a_1} \tag{3}$$

If the activity data of the bulk phase are known, the value of K' can be calculated at a given value of molecular exchange ratio: $r = V_{m,2}/V_{m,1}$ by means of computer iteration [32]-[35]. The applicability of Eq. (3) has been investigated by I. Dékány et al. in several publications [32]-[36]. It is revealed by the adsorption equilibrium diagrams that when the adsorption of a liquid pair consists of components with significantly different polarities, the value of the equilibrium constant K' decreases with increasing surface hydrophobicity of the different silicate surfaces covered by alkyl chains [38]-[43].

The material content of the adsorption layer is the adsorption capacity of the solid adsorbent, which may be determined in binary liquid mixtures if the so-called adsorption excess isotherm is known. Owing to adsorption, the initial composition of the liquid mixture, x_1^0, shifts to the equilibrium concentration x_1, where $n^s = n_1^s + n_2^s$ is the mass content of the interfacial phase (e.g., mmol/g). The difference, $x_1^0 - x_1 = \Delta x_1$, can be determined by simple analytical methods. The relationship between the reduced adsorption excess amount calculated from the change in concentration, $n_1^{\sigma(n)} = n^0(x_1^0 - x_1)$ and the material content of the interfacial layer is given by the Ostwald-de-Izaguirre equation [21]-[25]. In the case of purely physical adsorption of binary mixtures, the material content of the adsorption layer (n^s=n^o−n) for component 1 is illustrated by the following material balance [22]-[25]:

$$n^o x_1^o = n_1^s + (n^o - n^s) x_1 \tag{4}$$

$$n_1^\sigma = n^o (x_i^o - x_i) = n^o \Delta x_i \quad (i = 1, 2 \ldots) \tag{5}$$

where n^o is the total quantity of liquid mixture referred to unit mass of the adsorbent (e.g., mmole/g adsorbent), x_1^o is the mole fraction of the i-th component before adsorption, and x_1 is that in the equilibrium homogeneous liquid phase. The adsorption excess isotherms $n_1^\sigma = f(x_i)$ calculated in accordance with Eq. 1 can be classified into five basic types by the Schay-Nagy isotherm classification [22]-[24]. The Ostwald-de Izaguirre equation is obtained, free of assumptions, from the mass balance:

$$n^o (x_1^o - x_1) = n_1^{\sigma(n)} = n_1^s - n^s x_1 = n^s (x_1^s - x_1) \tag{6}$$

where $x_1^s = n_1^s/n^s$ is the mole fraction of the interfacial phase. According to Eq. (3), therefore, the excess isotherm $n_1^{\sigma(n)} = f(x_1)$ stems from a combination of the „individual" isotherms $n_1^s = f(x_1)$ and $n^s = f(x_1)$ [22]-[24].

Isotherms of types II, III and IV in the Schay-Nagy classification have the common characteristic that a fairly long section of the isotherm is practically linear [21-25]. For the linear section, we may write

$$n_1^{\sigma(n)} = a - b x_1 \tag{7}$$

Combining Eqs. (3) and (4):

$$a - b x_1 = n_1^s - n^s x_1 = n_1^s - (n_1^s + n_2^s) x_1 \tag{8}$$

Assuming that the intercepts of the linear sections are equal to the adsorption capacities of the components at the points $x_1 = 0$

and $x_2 = 1$, for the $x_1 = 0$ intercept $a = n_1^s$, while for the $x_2 = 1$ intercept $a - b = -n_2^s$ [21-25]. Since, in liquid sorption, the surface of the adsorbent is always completely covered, according to Williams the following equation can be written for the case of monomolecular surface coverage:

$$n_1^s a_{m,1} + n_2^s a_{m,2} = a_L^s \tag{9}$$

where $a_{m,1}$ and $a_{m,2}$ are the cross-sectional areas of the components 1 and 2, which can be calculated from the molar volumes of the components, and a_L^s is the equivalent specific surface area [29, 31, 42].

Eq. (6) can also be written in the following form:

$$n_1^s + r n_2^s = n_{m1,0}^s \tag{10}$$

where $n_{m,1,0}^s$ is the monomolecular adsorption capacity of pure component 1, and

$$a_L^s = n_{m1,0}^s a_{m,1} \tag{11}$$

According to Eqs. (10) and (11), the specific surface area of the adsorbent can be calculated from a knowledge of the adsorption capacities and the cross-sectional areas. The above method for determining the specific surface area has been applied to many systems in the literature, and it has been found that the specific surface areas calculated with the Schay-Nagy extrapolation method for non-swelling and disaggregating adsorbents agree very well with those calculated by the B.E.T. method [21]-[25].

The adsorption capacity $n_{1,0}^s$ of the pure component can be determined by the Everett-Schay (ES) method [21]-[28], [31]-[37]:

$$\frac{x_1 x_2}{n_1^{\sigma(n)}} = \frac{1}{n_{1,0}^s}\left[\frac{r}{S-1} + \frac{S-r}{S-1}\right] x_1, \tag{12}$$

For ideal adsorption from ideal solutions, S is constant [21]-[25]. The constancy of the separation factor in many other cases may result from compensation effects. From the linear dependence of $x_1 x_2 / n_1^{\sigma(n)}$ on x_1, we determine the value of $n_{1,0}^s$.

Given the knowledge of the adsorption excess isotherm $n_1^{\sigma(n)} = f(x_1)$, the so-called Individual isotherms are given by the following equations [21]-[25]:

$$n_1^s = \frac{r^* n_1^{\sigma(n)} + n_{1,0}^s x_1}{x_1 + r^* x_2} \tag{13}$$

$$n_2^s = \frac{n_{1,0}^s x_2 - n_1^{\sigma(n)}}{x_1 + r^* x_2} \tag{14}$$

where $n_{1,0}^s$ is the adsorption capacity relative to pure component 1 and $r^* = V_{m,2}/V_{m,1}$ is the ratio of the molar volumes of the components. In case of U-shaped excess isotherms, the adsorption capacity ($n_{1,0}^s$) can be determined from the linearized Everett-Schay function using Eq. (12) [21]-[25]. If the adsorption layer amount is known, the volume of the layer is obtained from the equation $V^s = n_{1,0}^s V m_1$, and the volume fraction of the adsorption layer can be calculated from the data of excess isotherms by the following equation:

$$\phi_1^s = \frac{n_1^s}{n_{1,0}^s} = \phi_1 + \frac{r^* n_1^{\sigma(n)} V_{m,1}}{V^s (x_1 + r^* x_2)} \tag{15}$$

If the specific surface area (a_L^s) of the particles is known, the thickness of the layer is $t^s = V^s/a^s$, which can be calculated from Eq. (15):

$$t^s = n_1^{-(n)} \left(\frac{V_{m,1}}{a^s x_1}\right)\left[\frac{\phi_1}{\phi_1^s - \phi_1)}\right] \tag{16}$$

where ϕ_1^s and ϕ_1 are the volume fractions of the adsorption layer and of the bulk phase, respectively, in adsorption equilibrium. The layer thickness t^s calculated according to the equation above is nearly constant. In non-ideal liquid mixtures, however, its value may depend on the composition of the bulk phase. In calculations of stability for disperse systems, knowledge of the thickness of the stabilizing adsorption layer is highly important [41]-[43].

2 Experimental

2.1 Materials

The TiO_2 nanoparticles were prepared using titanium(IV) isopropoxide (Fluka Chemica, pract.), purified water (Milli-Q, R = 18 MΩcm) and 2-propanol (Reanal Hungary, puriss). Concentrated hydrochloric acid (Reanal Hungary, pro anal.) and sodium hydroxide (Reanal Hungary, puriss) were used in the experiments. The TiO_2/clay mineral nanocomposites were prepared using Na-montmorillonite (EXM-838, D < 2μm, Süd-Chemie AG, Germany) as support material. The liquid sorption measurements were made from ethanol-cyclohexane binary liquid mixtures. In the photocatalytic efficiency studies the photodegradation of dichloroacetic acid (DCA, Aldrich, 99+%) was monitored.

2.2 Sample preparation

2.2.1 Preparation of the TiO_2 nanoparticles

The TiO_2 nanoparticles were prepared in aqueous media by means of sol-gel technique. A mixture of 174 mL titanium(IV) isopropoxide and 146 mL 2-propanol was added drop-wise into 660 mL Milli-Q water in 5 minutes under vigorous stirring in N_2 atmosphere. Due to hydrolysis a white, colloidal dispersion was formed, followed by the addition of 18 mL concentrated hydrochloric acid to the white slurry (pH $\sim$ 1). The product was held under thermostatic conditions (t = 50 ^{o}C) for 12 hours. After the hydrothermal treatment an almost transparent, stable $Ti(OH)_4/TiO_2$ sol was obtained.

2.2.2 Preparation of the $Ti(OH_4$-TiO_2/layer silicate nanocomposites

The original pH of the $Ti(OH)_4/TiO_2$ colloidal sol was around pH = 1. The calculated amount of the sol was added into the 1 % (g clay/100 mL of water) Na-montmorillonite suspension under vigorous stirring in 30 minutes. Different TiO_2/clay mass

ratios were used resulting in different compositions of the photocatalysts. The theoretical added TiO_2 contents were 20, 33, 50, 66, 75 w%. After 20 hours sedimentation, the heterocoagulated $Ti(OH)_4$-TiO_2/Na-montmorillonite precipitates were centrifuged at 10000 rpm for 30 minutes followed by washing of the solid phase using Milli-Q water. The twice-washed product was re-dispersed in Milli-Q water and the suspension was dialyzed for 90 hours to remove the residual electrolyte from the liquid phase. The dialyzed suspension was centrifuged again, and the solid phase was collected then dried at 50 ^{o}C in a hot box oven. These nanocomposite samples have the following notation: e.g., TiO_2 75/MA, where "75" means the semiconductor content of the nanocomposite in weight % units, "M" means the Na-montmorillonite support and "A" means the high acidic circumstances during preparation.

2.3 Measurement methods

The XRD experiments were carried out in a Philips X-ray diffractometer (PW 1930 generator, PW 1820 goniometer) with CuK-α radiation (λ = 0.1542 nm) 40 kV, 35 mA. The basal spacing (d_L) was calculated from the (001) reflection via the Bragg equation using the PW 1877 automated powder diffraction software.

Specific surface areas of TiO_2/Na-montmorillonite nanocomposites and TiO_2 samples were determined by a Micromeritics gas adsorption analyzer (Gemini Type 2375) at 77 K in liquid nitrogen. The adsorption and desorption branches of the isotherms were determined. Prior to measurements the samples were pretreated in vacuum (ca. 0.01 torr) at 393 K for 2 hours. The sample holder was loaded with ca. 0.1-0.3 g of samples. The adsorption isotherms were analyzed by means of the BET equation, the micropore volume data were determined with the de Boer's t-method, and the pore size distribution curves were analyzed by the Barret-Joyner-Halenda (BJH) method [44]. To determine the adsorption excess isotherms at 25$\pm$ 0.1^{o}C a Zeiss differential interferometer was used and 0.1 g catalyst was dispersed in 5 ml liquid mixtures in the whole composition range. After establishment of the adsorption equilibrium (24 hours) the equilibrium composition was determined by interferometry and the excess isotherms were calculated from Eqs. (4-6).

For the band gap energy determination the optical properties of the composites were determined using an Ocean Optics Chem2000 diode array spectrophotometer.

The effective titanium content of the TiO_2 containing nanocomposites was determined by inductively coupled plasma (ICP) spectrometry using a Jobin-Yvon 24 sequential ICP-OES analyzer.

The photodegradation of the dichloroacetic acid, the model pollutant, was monitored by pH-stat titration. Constant ionic strength (I = 10 mmol/l, KNO_3) was used in all experiments. The reaction vessel was thermostated during the irradiation (t = 25^{o}C). All experiments were performed in 200 mL suspension in which the DCA concentration was 1 mmol/l. The irradiation procedure was carried out in a home-built system and the reaction was controlled by home-written software. Photocatalytic experiments were carried out in a thermostated glass reactor equipped with an external pH measurement cell. The suspension was continuously circulated at a constant rate by means of a peristaltic pump. The instantaneous value of the pH of the suspension was measured on-line. The schematic diagram of the reactor is represented on the Fig. 1. The suspension of the DCA solution and the given catalyst were introduced into a glass reaction vessel (2), then transferred to a photoreactor box (8) equipped with a 150W high pressure mercury lamp (3). The suspension was stirred continuously using a magnetic stirrer (1). A small amount of the total volume of the suspension was continuously extracted and returned using a peristaltic pump (not shown in the diagram) into the external measuring cell (4) equipped with a combined pH-electrode. In all cases, air was introduced into the suspensions (9) at a constant flow rate (1 mL/min) during the illumination. The raw signal generated by the pH-electrode was converted by a D/A converter (5) and then processed by the PC (6), which controlled the automatic burette (7) by means of the home-made software noted in ref. [44].

3 Results and Discussion

3.1 Structural properties of TiO_2/layer silicate nanocomposites

X-ray diffractograms in the 2Θ angle range 20-30^o characteristic of series M were taken after drying the samples at 50^{o}C (Fig. 2). The reflections found in this range are characteristic of the structure of titanium dioxide. The peaks at 25.3° (2Θ) and 27.5° (2Θ) correspond to the anatase (101) and rutile (110) phases, respectively. The intensities of the reflections at 25.3^o(2Θ) increase with increasing TiO_2 content, demonstrating that, in the course of sol preparation, only the anatase crystalline modification of TiO_2 was formed, since the reflection characteristic of rutile (2Θ=27.5^o) is missing. For samples prepared by sol-gel synthesis the anatase reflection calculated from the Bragg equation is d_{101} = 3.52 Å, whereas the average particle diameter calculated from the half-width values of the same peaks by the Scherrer equation is 3.6-4.0 nm. The reflections seen in the small angle region of the diffractograms are characteristic of the silicate layer used as support, and their intensities decrease with increasing composite TiO_2 content. Basal spacings (d_L), calculated with the Bragg equation from the reflection characteristics of the intercalation structure in the small angle region (1-15^o (2Θ)), were found at 2Θ=2.5^o and are listed in Table 1. Based on these data, the average basal spacing values lie in the range of 3.4-3.6 nm. The particle diameter calculated using this value, $d_{TiO_2} = d_L - d_{TOT}$ (where d_{TOT} = 0.96 nm, i.e., the thickness of a single lamella of Na-montmorillonite generated by tetrahedral-octahedral-tetrahedral planes) is 2-3 nm.

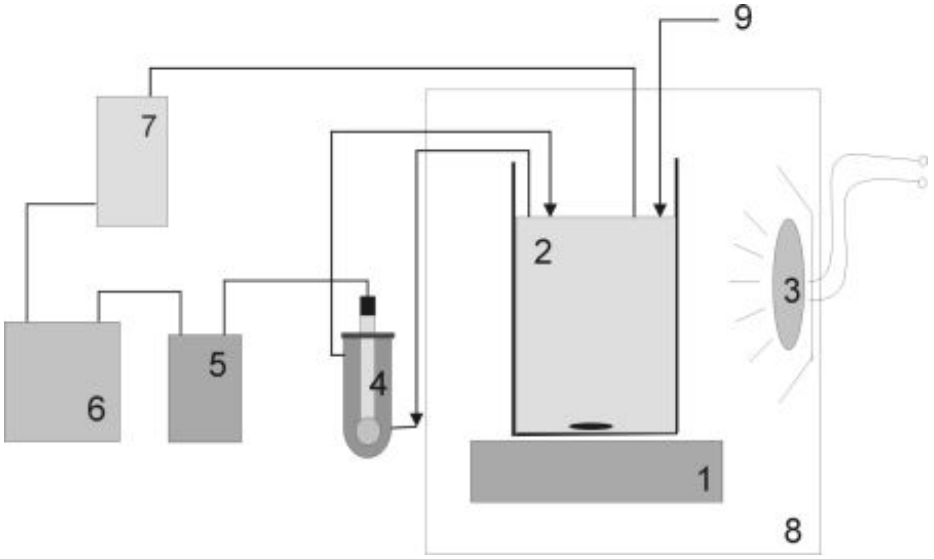

(1: magnetic stirrer, 2: glass reaction vessel and suspension, 3: high-pressure mercury lamp, 4: external measuring cell with combined pH-electrode, 5: D/A converter, 6: computer, 7: automatic burette, 8: photoreactor box, 9: air inlet)

Fig. 1. Schematic arrangement of the measurement systems for photocatalytic reactions.

Tab. 1. Structural and optical properties of the photocatalyst samples

sample	(1) TiO_2 content (%)	(2) d_L (nm)	(3) λ_g (nm)	(4) E_g (eV)
sol-gel TiO_2	100	–	397	3.12
sol-gel TiO_2 (400 ^oC)	100	–	477	2.60
TiO_2 75/MA	69.01	3.46	378	3.28
TiO_2 66/MA	63.51	3.48	377	3.29
TiO_2 50/MA	47.41	3.49	375	3.30
TiO_2 33/MA	29.42	3.50	373	3.32
TiO_2 20/MA	18.91	3.49	367	3.38
Na-montmorillonite	0	1.15	-	-

(1) TiO_2 content determined by ICP measurement
(2) Determined by XRD measurements and calculated from the Bragg equation
(3) Determined from absorbance measurement of the dilute (0.01-0.05 g/100 mL) suspensions
(4) Calculated by $\lambda_g = 1240/E_g$, where E_g is the band gap energy in eV units

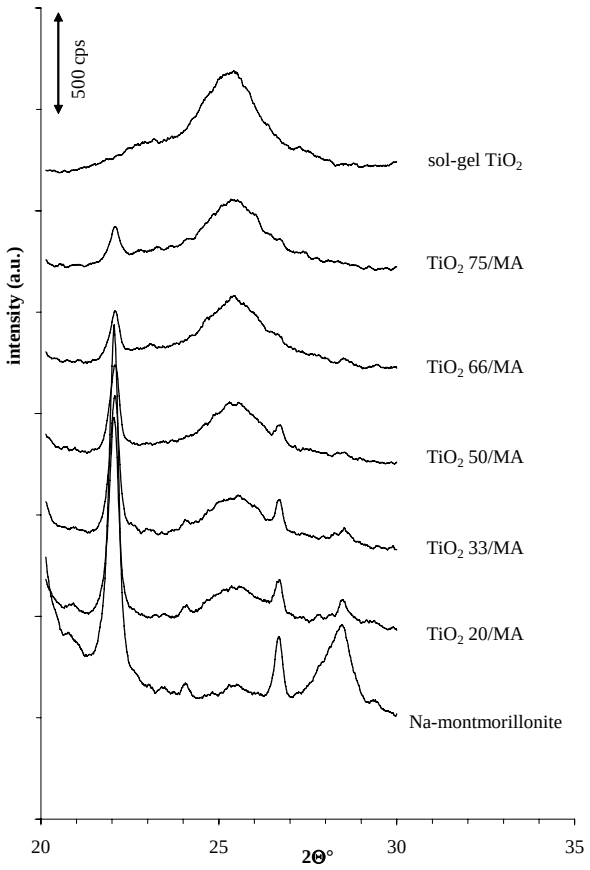

Fig. 2. XRD pattern of titanium-dioxide and in titania-intercalated montmorillonite.

The specific surface areas and the porosities of the samples were determined by N_2 adsorption measurements. Isotherms were analyzed by the BET method; the specific surface areas of the samples were determined and are listed in Table 2. The specific surface area of the original layer silicate used as support (ca. 28 m^2/g) increases gradually with increasing TiO_2 content, because TiO_2 particles are incorporated between the lamellae. It is also seen that pure TiO_2 prepared by the sol-gel method has a high specific surface area (ca. 270 m^2/g). We suppose that the high specific surface area of composites is the cumulative

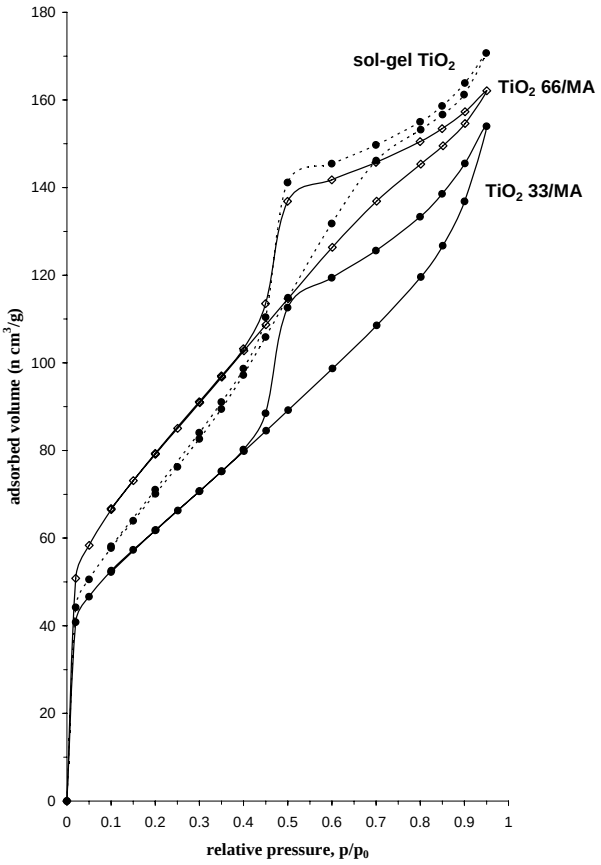

Fig. 3.a. Nitrogen adsorption isotherms at 77 K on different TiO_2-montmorillonite composites and the titania photoctalyst prepared by sol-gel method.

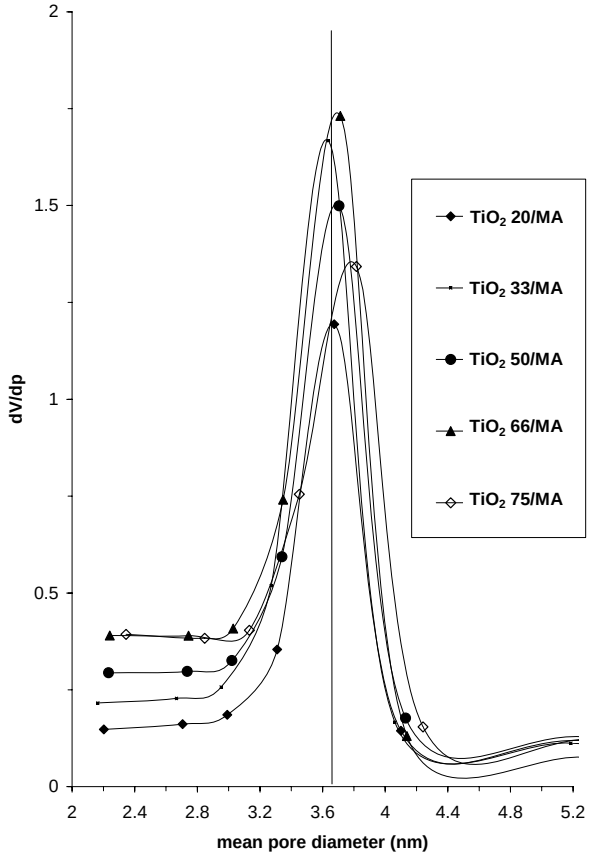

Fig. 3.b. Calculated pore size distribution functions using nitrogen adsorption measurements on different TiO_2-montmorillonite composites and the titania prepared by sol-gel method.

result of two effects. On the one hand, pillaring the lamellae of layer silicates generates a layered nanocomposite material with a larger internal surface; on the other hand, porous TiO_2 located in the interlamellar space also contributes to the increase in specific surface area. Based on previous results and experience, this increase in specific surface area can be attributed to a modification of the structure of the layer silicate support in the highly acidic medium due to dissolution of Al ions from the crystal lattice. Taking into consideration that particle synthesis itself takes place under extremely acidic conditions (pH<1), it can be concluded that the increase in specific surface area is a result of the increase in the surface and porosity of the clay mineral [44]. Fig. 3.a shows some of the nitrogen adsorption isotherms at 77 K, namely the samples with 33%, 66% TiO_2 content and of sol-gel TiO_2. All three isotherms clearly belong to type IV of the classification according to Brunauer, Emmett and Teller (BET), characteristic of porous adsorbents [22,24]. The hysteresis loops indicate high porosity. It can be established on the basis of the shape of the hysteresis loop that in each sample the size distribution of pores is only slightly polydisperse. The pores in the samples fall into the range of micro- and mesopores. The pore size distribution was calculated from the appropriate section of the desorption branch of each isotherm using the Barrett, Joyner, Halenda (BJH) method [22,24,44]. In the case of the TiO_2/MA series, the maximum of the pore size distribution curve fluctuated around a given value (3.6-3.7 nm) (see Fig. 3.b). The most characteristic pore diameters lay in the range 3-4 nm for both series. These data are in good agreement with the values of d_L measured by X-ray diffraction Table 1. The sol-gel TiO_2 sample also exhibits porous character: adsorption hysteresis is observed in its isotherm as well.

Tab. 2. Results of the nitrogen adsorption experiments

sample	$^{(1)}a^S_{BET}$ m^2/g	$^{(2)}a^S_{ext}$ m^2/g	$^{(2)}a^S_{mp}$ m^2/g	$^{(2)}V_{mp}$ cm^3/g	$^{(3)}V^S_{max}$ cm^3/g (STP)
Na-montmorillonite	28	41	6.3	0.0030	59.5
TiO_2 20/MA (50 ^{o}C)	153	143	9.49	0.0041	128.4
TiO_2 33/MA (50 ^{o}C)	198	193	4.66	0.0012	143.4
TiO_2 50/MA (50 ^{o}C)	240	–	–	–	157.3
TiO_2 66/MA (50 ^{o}C)	251	–	–	–	156.9
TiO_2 75/MA (50 ^{o}C)	270	–	–	–	176.6
sol-gel TiO_2 (50 ^{o}C)	268	–	–	–	149.4

(1) calculated by the BET equation

(2) determined by the deBoer's t-plot method

(3) maximum adsorbed volume data is given in normal units of cm^3/g

The adsorption isotherms belong to type II in the Schay-Nagy classification. That means the ethanol will be adsorbed preferentially on the polar surface of the composite adsorbent. The slopes of the isotherms depend on the TiO_2 content of the composite samples.

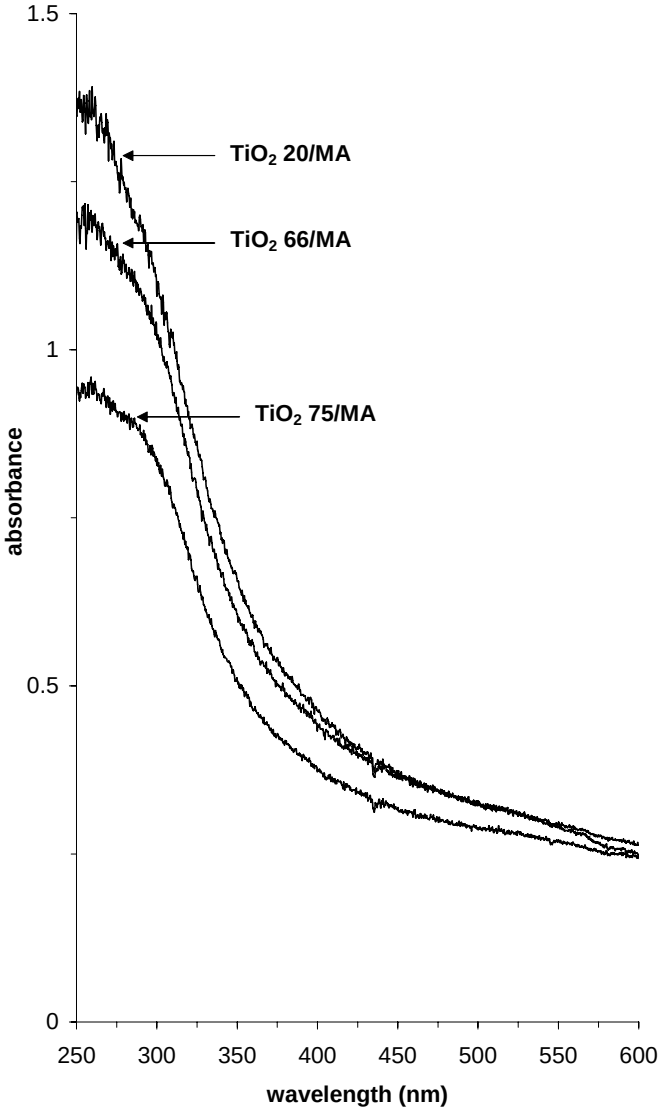

Fig. 4. UV-Vis absorption spectra of TiO_2-montmorillonite composites.

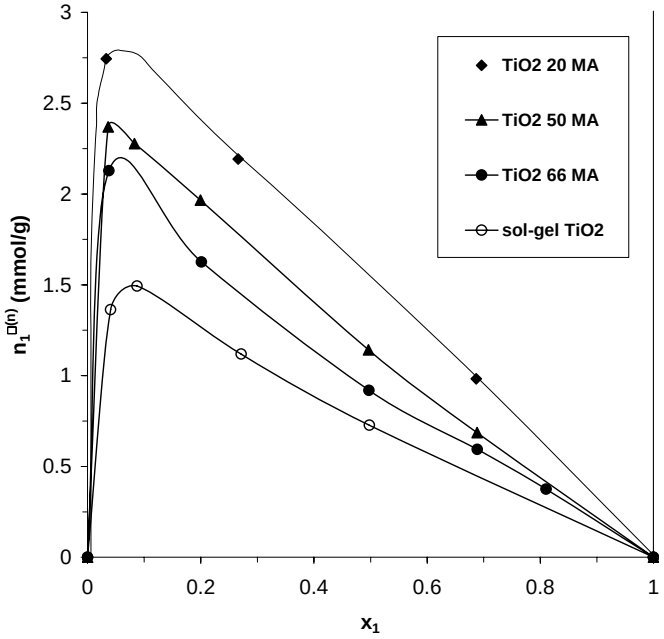

Fig. 5. Adsorption excess isotherms in ethanol(1)-cyclohexane(2) binary liquid mixtures on the different photocatalysts.

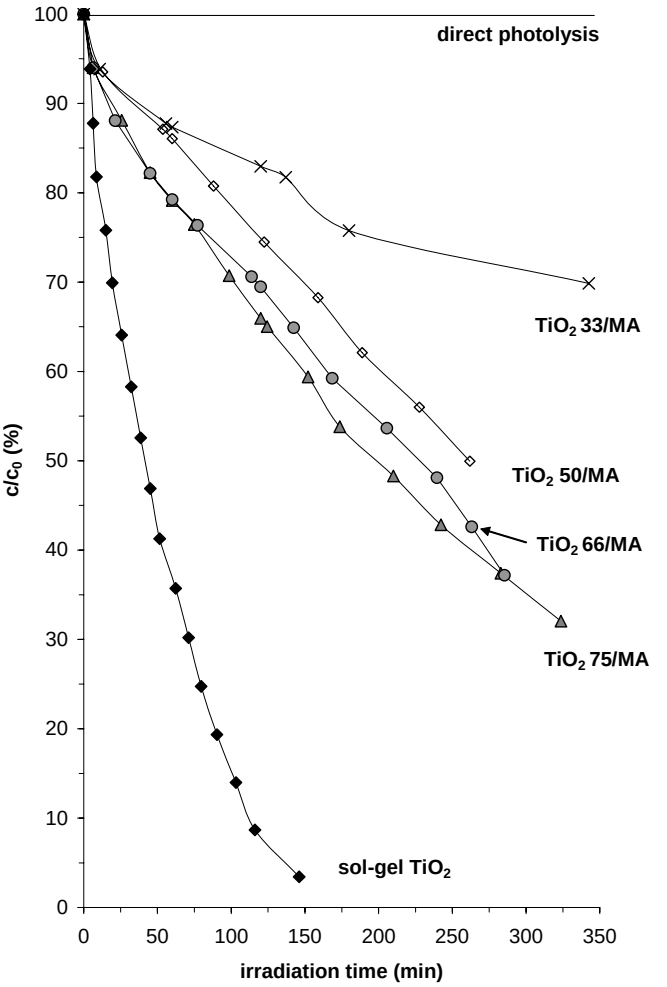

Fig. 6. Photo-oxidation process of DCA on different photocatalyst composites.

The calculated adsorption capacities, using Eqs. (7) and (12), agree well with each other. The specific surface area calculated from the N_2 adsorption data is nearly the same for the TiO_2 66 MA sample. The TiO_2-montmorillonite composites show higher equivalent specific surface area at low TiO_2 content than the BET surface area, because it is possible to build up a second adsorption layer for ethanol in the confined space of the layer silicate support. If the TiO_2 content is higher, the liquid sorption capacity is lower, because the interlamellar free space between the TiO_2 pillars is also smaller. That means that ethanol does not have access between the layers, and only nitrogen molecules can be incorporated into the small pores. The average adsorption layer thickness ranges between 0.47 and 0.53 nm, showing the bilayer structure formation of ethanol in the interlamellar confined space as calculated from Eq. (16) (see Table 3).

The band gap energy (E_g, given in eV) of nanocomposites and pure sol-gel TiO_2 was determined on the basis of UV-Vis photometric assays in order to identify the wavelengths that can excite TiO_2/montmorillonite nanocomposites for the purposes of photocatalysis. Typical light absorption spectra of some nanocomposites, which were used for calculating λ_g (in nm) listed in Table 1, are shown in Fig. 4. In many previous publications a value of E_g = 3.2 eV was determined for bulk TiO_2 [3]-[8, 44].

Tab. 3. Comparison of the surface areas from BET equation, Everett-Schay function and Schay-Nagy (S-N) extrapolation method

Photocatalyst sample	Slope of Eq. (12) $= 1/n^s_{1,0}$	$n^s_{1,0}$ (mmol/g)	$n^{s,}_1$ (mmol/g)	a_L (m^2/g)	a_L (m^2/g)	a^s_{BET} (m^2/g)	t^s (nm)
	Calculated after Eq. (12)		From S-N extrapolation Eq.(7)	Eq(12)	From S-N extrapolation Eq.(7)		From Eq.(16)
TiO_2 20/MA	0.3111	3.2144	3.06	386	367	153	0.475
TiO_2 33/MA	0.3649	2.7405	2.67	329	320	198	0.483
TiO_2 50/MA	0.4380	2.2831	2.45	274	294	240	0.487
TiO_2 66/MA	0.5202	1.9223	2.06	231	247	251	0.535
TiO_2 75/MA	0.5563	1.7976	1.77	216	212	270	0.491
Sol-gel TiO_2	0.6744	1.4828	1.53	178	183	268	0.515
Na-montm.	0.5320	1.8797	1.92	225	230	47	0.512

Cross section area of ethanol: A_m = 120 m^2/mmol

Tab. 4. Photocatalytic characterization of the samples

Sample	TiO_2 content	0.01 M KOH consumption % (ml)	produced H^+ (mmol) after 60 min	produced H^+/g catalyst (mmol/g)	produced H^+/g TiO_2 (mmol/g)	Conversion after 60 min irradiation (%)
sol-gel TiO_2	100	10.95	0.1221	0.6105	0.6105	63.06
TiO_2 75/MA	69.0	3.59	0.0389	0.1945	0.2818	20.85
TiO_2 66/MA	63.5	3.56	0.0387	0.1935	0.3047	20.76
TiO_2 50/MA	47.4	2.21	0.0260	0.1297	0.2743	13.93
TiO_2 33/MA	29.4	2.11	0.0235	0.1175	0.3994	12.66
TiO_2 20/MA	18.9	0	0	0	0	0
Na-montm.	0	0	0	0	–	0
direct photolysis	0	0	0	0	0	0

The Table 1 also reveals that the value of E_g for calcinated sol-gel TiO_2 is further decreased, which can be explained by an increase in the extent of crystallinity and in particle size of TiO_2. The optical properties of TiO_2 nanoparticles on the acid-treated support are closer to those of pure TiO_2 prepared by the sol-gel method.

Table 3 compares the solid-gas and solid-liquid adsorption data. The specific surface areas calculated with the two different methods agree well with each other. The liquid sorption isotherms show different slopes because the adsorption capacities calculated for the preferentially adsorbed polar component ethanol increase with the free interlamellar space of TiO_2-montmorillonite photocatalyst. This interlamellar adsorption space is responsible for the accessibility of adsorbed DCA molecules for photocatalytic decomposition (see Fig. 5).

3.2 Photocatalytic properties

The photocatalytic efficiency of TiO_2-containing nanocomposites was tested in the degradation of dichloroacetic acid (DCA). The reaction of DCA in the presence of UV light and catalyst is the following:

$$CHCl_2COO^- + O_2 \xrightarrow{h\nu,TiO_2} 2CO_2 + H^+ + 2Cl^-$$

The amount of acid generated by the photocatalytic reaction can be monitored continuously by detecting the change in pH. The results can be represented in degradation curves such as shown in Fig. 6 (initial values are taken as 100%). The figure displays the results obtained with the sample series TiO_2 /MA and with direct photolysis. In Table 4 the numerical values of degradation data are listed, namely the amount of alkali solution added, the amount of acid formed (in mmol), the amount of acid formed normalized to catalyst amount and to net TiO_2 content and conversion.

An increase in the absolute value of catalytic activity with increasing TiO_2 content can be observed. In spite of the fact that the absolute value of efficiency does indeed increase with increasing TiO_2 content of the catalysts used, a different picture emerges when the results are normalized with respect to pure TiO_2. When the catalytic efficiency is normalized to the mass of the TiO_2 content, different results are obtained. The calculated data are presented in Table 4; the data of series TiO_2/MA are represented in Fig. 7. When the rate of degradation is normalized with respect to the mass of TiO_2 it is can be seen that the highest efficiencies (0.3994 mmol $H^+/gTiO_2$) are attained by catalyst TiO_2 33/M. Comparing the rate of photo-oxidation with the liquid adsorption data, the highest specific surface area (320 m^2/g) of composite catalyst for liquid sorption is given for this sample, because the accessibility for DCA molecules is also highly favourable in this confined adsorption space (see Table 3).

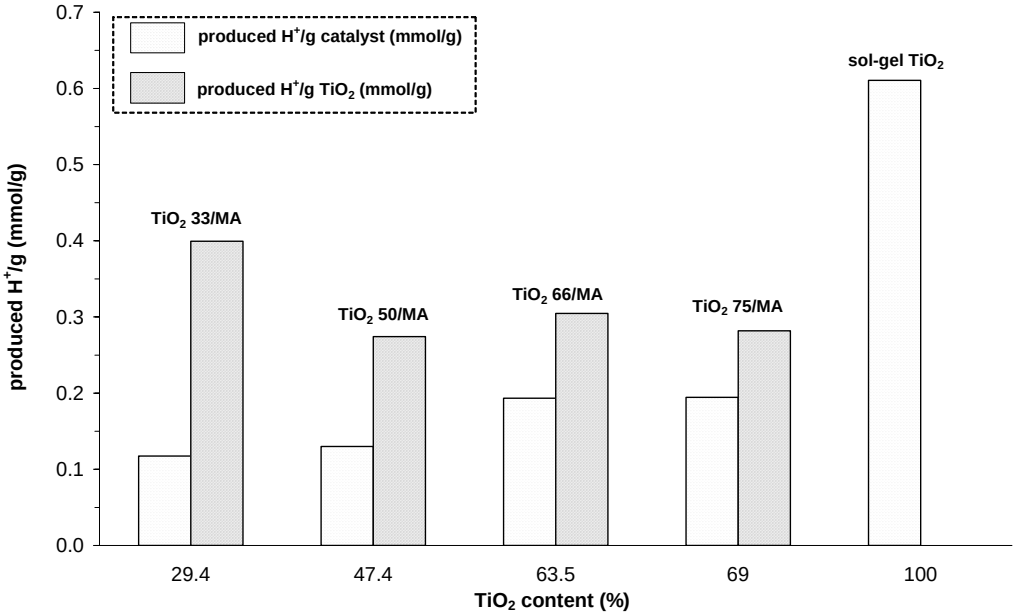

Fig. 7. Comparison of the different photocatalyst samples for DCA decomposition, calculated for pure TiO_2 and catalyst amount respectively.

4 Conclusion

The calculated structural and adsorption characteristics of TiO_2/layer silicate nanocomposites were compared to the low temperature nitrogen adsorption and ethanol-cyclohexane liquid mixture adsorption data. Gas adsorption shows greater access to the intercalated TiO_2 nanoparticles incorporated between the silicate layers. The rates of photocatalytic oxidation of the DCA molecules are correlated to the interfacial layer properties in the confined space deduced from the liquid sorption experimental data.

References

1 **Barringer EA, Bowen HK**, *High-purity, monodisperse TiO_2 powders by hydrolysis of titanium tetraethoxide, 1. Synthesis and physical-properties*, Langmuir **1** (1985), 414-420, DOI 10.1021/la00064a005.

2 **Nishimoto SI, Ohtani B, Kajiwara H, Kagiya T**, *Correlation of the crystal-structure of titanium-dioxide prepared from titanium tetra-2-propoxide with the photocatalyic activity for redox reactions in aqueous propan-2-ol and silver salt-solutions,* J. Chem. Soc., Faraday Trans.1 **81** (1985), 61-68, DOI 10.1039/F19858100061.

3 **Ogawa M, Kuroda K**, *Preparation of inorganic-organic nanocomposites through intercalation of organoammonium ions into layered silicates,* Bull. Chem. Soc. Japan. **70** (1997), 2593-2618, DOI 10.1246/bcsj.70.2593.

4 **Scolan E, Sanchez C**, *Synthesis and characterization of surface protected nanocrystalline titania particles*, Chem. Mater. **10** (1998), 3217-3223, DOI 10.1021/cm980322q.

5 **Pelizzetti E, Minero C, Borgarello E, Tinucci L, Serpone N**, *Photocatalytic activity and selectivity of titania colloids and particles prepared by the sol-gel technique – Photooxidation of phenol and atrazine,* Langmuir **9** (1993), 2995-3001, DOI 10.1021/la00035a043.

6 **Minero C, Pelizzetti E, Malato S, Blanco J**, *Large solar plant photocatalytic water decontamination: Effect of operational parameters*, Solar Energy **56** (1996), 421-428, DOI 10.1016/0038-092x(96)00029-1.

7 **Mills A, Wang JS**, *Photomineralisation of 4-clorophenol sensitized by TiO_2 thin films*, J. Photochem. Photobiol. A **118** (1998), 53-63, DOI 10.1016/S1010-6030(98)00348-7.

8 **Matsushita SI, Miwa T, Tryk DA, Fujishima A**, *New mesostructured porous TiO_2 surface prepared using a two-dimensional array-based template of silica particles*, Langmuir **14** (1998), 6441-6447, DOI 10.1021/la9811062.

9 **Wang CC, Ying JY**, *Sol-gel synthesis and hydrothermal processing of anatase and rutile titania nanocrystals*, Chem. Mater. **11** (1999), 3113-3120, DOI 10.1020/cm990180f.

10 **Brown GT, Darwent JR**, *Methyl-orange as a probe for photooxidation reactions of colloidal TiO_2*, J. Phys. Chem. **88** (1984), 4955-4959, DOI 10.1021/j150665a032.

11 **Xu Y, Langford CH**, *Photoactivity of titanium dioxide supported on MCM41, zeolite X, and zeolite,* J. Phys. Chem. B **101** (1997), 3115-3121, DOI 10.1021/jp962494l.

12 **Yamanaka S, Nishihara T, Hattori M, Suzuki Y**, *Preparation and properties of titania pillared clay*, Materials Chemistry and Physics **17** (1987), 87-101, DOI 10.1016/0254-0584(87)90050-2.

13 **Ooka C, Akita S, Ohashi Y, Horiuchi T, Suzuki K, Komai S, Yoshida H, Hattori T**, *Crystallization of hydrothermally treated TiO_2 pillars in pillared montmorillonite for improvement of the photocatalytic activity*, J. Mater. Chem. **9** (1999), 2943-2952, DOI 10.1039/a901421g.

14 **Choy JH, Park JH, Yoon JB**, *Multilayered SiO_2/TiO_2 nanosol particles in two-dimensional aluminosilicate catalyst support*, J. Phys. Chem. B **102** (1998), 5991-5995, DOI 10.1021/jp9815863.

15 **Anderson C, Bard AJ**, *Improved photocatalytic activity and characterization of mixed TiO_2/SiO_2 and TiO_2/Al_2O_3 materials*, J. Phys. Chem. B **101** (1997), 2611-2616, DOI 10.1021/jp9626982.

16 **Sterte J**, *Synthesis and properties of titanium oxide cross-linked montmorillonite*, Clays and Clay Minerals **34** (1986), 658-664, DOI 10.1346/CCMN.1986.0340606.

17 **Ding Z, Zhu HY, Greenfield PF, Lu GQ**, *Characterization of pore structure and coordination of titanium in TiO_2 and SiO_2-TiO_2 sol-pillared clays*, J. Coll. Interf. Sci. **238** (2001), 267-272, DOI 10.1006/jcis.2001.7504.

18 **Ding Z, Zhu HY, Lu GQ, Greenfield PF**, *Photocatalytic properties of titania pillared clays by different drying methods*, J. Coll. Interf. Sci. **209** (1999), 193-199, DOI 10.1006/jcis.1998.5857.

19 **Puma GL, Yue PL**, *Comparison of the effectiveness of photon-based oxidation processes in a pilot falling film photoreactor*, Environ. Sci. Technol. **33** (1999), 3210-3216, DOI 10.1021/es9811795.

20 **Vinodgopal K, Kamat P**, *Enhanced rates of photocatalytic degradation of an azo-dye using SnO_2/TiO_2 coupled semiconductor thin films*, Environ. Sci. Technol. **29** (1995), 841-845, DOI 10.1021/es00003a037.

21 **Nagy LGy**, *Periodica Polytechnica* **7** (1962), 75-91.

22 **Schay G**, *Surface and Colloid Science* (Matijevic E, ed.), Vol. 2, Wiley, London, 1969.

23 **Everett DH**, *Thermodynamics of adsorption from solution. Part 1.—Perfect systems Thermodynamics of adsorption from solution. Part 2.Imperfectsystems*, Trans. Faraday Soc. **60** (1964), 1803-1809, DOI 10.1351/pac197648040393.

24 **Kipling J J**, *Adsorption from Solutions of Non-Electrolytes*, Academic Press, London, 1965.

25 **Schay G**, *A Comprehensive Presentation of the Thermodynamics of Adsorption Excess Quantities*, Pure Appl. Chem. **48** (1976), 393-400, DOI 10.1039/TF9646001803.

26 **Myers AL, Sircar S A**, *Thermodynamics Consistency Test for Adsorption of Liquids and Vapours on Solids*, J. Phys. Chem. **76** (1972), 3412-3415, DOI 10.1021/j100667a020.

27 **Zettlemoyer A Z, Young G J, Chessick J J**, *Studies of the Surface Chemistry of Silicate Minerals. III. Heats of Immersion of Bentonite in Water*, J Phys. Chem. **59** (1955), 962-970, DOI 10.1021/j150531a034.

28 **Everett D H**, *Thermodynamics of interfacial phenomena*, Pure Appl. Chem. **53** (1981), 2181-2192, DOI 10.1351/pac198153112181.

29 **Dékány I, Szántó F, Nagy LG, Schay G**, *Sorption and immersional wetting properties of palygorskite and its hexadecylpyridinium derivatives*, J. Colloid Interface Sci. **93** (1983), 151-165, DOI 10.1016/0021-9797(83)90394-6.

30 **Dékány I, Szántó F, Nagy L G**, *Sorption and immersional wetting on clay minerals having modified surfce, I. Surface properties of nonswelling clay mineral organocomplexes,* J Colloid Interface Sci. **103** (1985), 321-332, DOI 101016/0021-9797(85)90110-9.

31 _____, *Sorption and immersional wetting on clay minerals having modified surface, II. Interlamellar sorption and wetting on organic montmorillonites*, J. Colloid Interface Sci. **109** (1986), 376-386, DOI 10.1016/0021-9797(86)90316-4.

32 **Dékány I, Zsednai Á, László K, Nagy L G**, *Enthalpy of displacement of binary liquid mixtures on solid surfaces, II. Analysis of S-shaped excess isotherms*, Colloids Surfaces A. **23** (1987), 41-56.

33 **Dékány I, Ábrahám I, Nagy L G, László K**, *Enthalpy of displacement of binary liquid mixtures on solid surfaces, III.: Determination of the adsorption capacity from calorimetric and adsorption data*, Colloids and Surfaces A **23** (1987), 57-68.

34 **Regdon I, Király Z, Dékány I, Lagaly G**, *Microcalorimetric studies of S/L interfacial layers: thermodynamic parameters of the adsorption of butanol-water on hydrophobized clay minerals*, Progress Colloid Polymer Sci. **109** (1998), 214-220, DOI 10.1007/BFb0118173.

35 **Dékány I, Marosi T, Király Z, Nagy LG**, *Surface modification and surface thermodynamic potential functions at the S/L interface*, Colloids Surfaces A **49** (1990), 81-93, DOI 10.1016/0166-6622(90)80094-K.

36 **Dékány I, Zsednai Á, Király Z, László K, Nagy LG**, *Enthalpy of displacement of binary liquid mixtures on solid surfaces, I. Analysis of U-shaped isotherms* **19** (1986), 47-59.

37 **Dékány I, Szántó F, Nagy L G, Fóti G**, *Adsorption of liquid mixtures on bentonite and organophilic bentonite*, J. Colloid Interface Sci. **50** (1975), 265-271, DOI 101016/0021-9797(75)90229-5.

38 **Dékány I, Szántó F, Nagy L G**, *Selective liquid sorption and structural properties of montmorillonite and its hexadecypyriinium derivatives*, J. Colloid Polymer Sci. **256** (1978), 150-160, DOI 10.1007/BF01679173.

39 **Dékány I, Nagy LG, Schay G**, *Effect of surface modification on solid-liquid interfacial adsorption of mixtures*, J. Colloid Interface Sci. **66** (1978), 197-200, DOI 10.1016/0021-9797(78)90202-3.

40 **Dékány I, Szántó F, Nagy LG**, *Wetting and adsorption on organophilic illites and swelling montmorillonites in methanol-benzene mixtures*, J. Colloid Polymer Sci. **266** (1988), 82-96, DOI 10.1007/BF01451536.

41 **Dékány I, Nagy LG**, *Immersional wetting and adsorption displacement on hydrophilic/hydrophobic surfaces*, J. Colloid Interface Sci. **147** (1991), 119-127, DOI 10.1016/0021-9797(91)90140-4.

42 **Dékány I**, *Liquid adsorption and immersional wetting on hydrophilic/ hydrophobic solid surfaces*, Pure Appl. Chem. **64** (1992), 1499-1509, DOI 10.1351/pac199264101499.

43 _____, *Adsorption and immersional wetting on hydrophilic and hydrophobic silicates*, Studies in Surface Science and Catalysis (A.Dabrowski, V.A.Tertykn V A, eds.), Vol. 99, Elsevier Sci. B.V. Amsterdam. Ch. 3.9, 1996, pp. 879-89.

44 **Kun R, Mogyorósi K, Dékány I**, *Synthesis and structural and photocatalytic properties of TiO_2/montmorillonite nanocomposites*, Appl. Clay Sci. **32** (2006), 99-110, DOI 10.1016/j.clay.2005.09.007.